INDIRECT EVALUATION OF CONTACT PRESSURE BETWEEN FRAME AND STATOR CORE OF SELF-COOLED ELECTRIC MOTORS BY MEANS OF FINITE ELEMENT MODELS AND STRAIN GAUGES.

Rafael Beck, rafaelb@weg.net
Vinícius S. Gonçalves, viniciusg@weg.net
WEG Electric Equipments S.A.
Waldemar Grubba Avenue, 3000 – PO. Box 420
Zip code: 89256-900, Jaraguá do Sul, Santa Catarina, Brazil
Phone: +55 47 32764803 / Fax: +55 47 32764931

Abstract. *The existing competitive scene demands for products which have higher quality amongst lower final prices. These are translated into meet customer's requirements at the lowest possible cost. For this, the deep product knowledge is fundamental. Examples of requirements are vibration and noise levels in self cooled electric motors. According to Schlensok et al. (2008) and Ishibashi et al. (2010), these characteristics, among others factors, are closely related to the contact pressure between the electric motor frame and its stator core. Thus, the purpose of this study is to quantify indirectly the contact pressure between these components by means of finite element models that use as data the superficial strains of the frame, obtained by strain gauges during the assembly process. Furthermore, experimental modal analysis are made in order to assist the numerical model adjust. The methodology includes a special tooling in the internal diameter of two frames of identical electric motors, in the way that very distinct values of contact pressure are obtained. Identical tooling places are previewed for the strain gauges in both frames. The numerical models use the symmetry of the problem to reduce processing costs. In the region where the strain gauges are attached, the geometry is manipulated to describe the strain gauge length, allowing more freedom in the process of mesh refinement and consequently, more accurate strain values. The convergence of the model leads to the contact pressure between the components, that is, the radial stresses produced on the contact surface. Preliminary results show that the residual deformations of the frame after the tooling process exert direct influence in the experimental results. The numerical model doesn't consider such deformations and asymmetries, resulting in some divergences between numerical and experimental results.*

Keywords*: Contact pressure, strain gauges, finite elements.*

1. INTRODUCTION

The existing competitive scene demands for products which have higher quality amongst lower final prices. These are translated into meet customer's requirements at the lowest possible cost. For this, the deep product knowledge is fundamental. Examples of requirements are vibration and acoustic noise levels in self cooled electric motors, forced continually to lower levels. The vibration and acoustic noise levels, among other factors, are directly related to the mechanical linkage between the electric motor frame and its stator core. It is expected that the larger the area in contact and higher the contact pressure between these components, below allowable stresses values, lower will be the vibration and acoustic noise levels.

According to Ishibashi *et al*. (2010), the frame shape and the number of points in contact between frame and stator core are determinant factors of the stator core natural frequencies. If these frequencies coincide with or are close to the frequencies of magneto-motive forces, it will occur the resonance phenomenon, which will amplify the vibration levels of the stator core, which in turn, are responsible for the increase of the acoustic magnetic noise in the electric motor, Alger (1970), Ishibashi *et al*. (1998). Schlensok *et al*. (2008), analyzed induction machines dynamic behavior regarding the mechanical linkage type between frame and stator core. Their models consider two linkage types. The first represents the contact stiffness by means of helical springs, and the second, which consider interference linkage. For each of the models, were obtained the deformation amplitudes on the frame external diameter as function of the ensemble natural frequencies. It was observed that as the number of springs became larger, the deformations on the frame became lower, and by the end, for an interference linkage, which is equivalent to an infinite number of springs, one can achieve the lowest deformation values.

Errors are inherent to the production process and must be known to be controlled. In the tooling process of the frame internal diameter, occur errors that tend to generate an elliptical shape on it, deviating it from a perfect cylinder. These errors are due to differences in the frame stiffness point to point. As an example, the feet aggregate stiffness to the frame's body, so one can expect that in the tooling process, this region will suffer lower deformations if compared to other regions. Due to these errors, there are variations in the contact pressure between frame and stator core throughout the contact surface length. In a critical case, it might be regions of the frame that in fact, are not in contact with the stator core. This reflects on the strains measured by the strain gauges placed on the frame. Therefore, knowing the errors is fundamental for the finite element model validation.

2. INTERFERENCE LINKAGE

Among the existing types of assembly and fixation, the simplest, cleanest and less expensive, maybe is the interference linkage type. Figure 1 presents the assembly of two hollow cylinders by interference. In this situation, a contact pressure p arises between them and causes a radial stresses $\sigma_r = -p$ in each cylinder on the contact surface, located in the transition radius R. The radius r_i and r_o are the internal radius of the internal cylinder and the external radius of the external cylinder, respectively. The tangential stress in the internal cylinder on the contact surface, according Shigley *et al.* (2005), is given by

$$(\sigma_t)_i = -p\frac{R^2 + r_i^2}{R^2 - r_i^2}. \tag{1}$$

Likewise, the tangential stress in the external cylinder on the contact surface is

$$(\sigma_t)_o = p\frac{r_o^2 + R^2}{r_o^2 - R^2}. \tag{2}$$

The total radial interference δ between the cylinders is given by

$$\delta = |\delta_i| + |\delta_o|, \tag{3}$$

where $|\delta_i|$ and $|\delta_o|$ are the variations in the internal and external cylinders radius, respectively, around the nominal value.

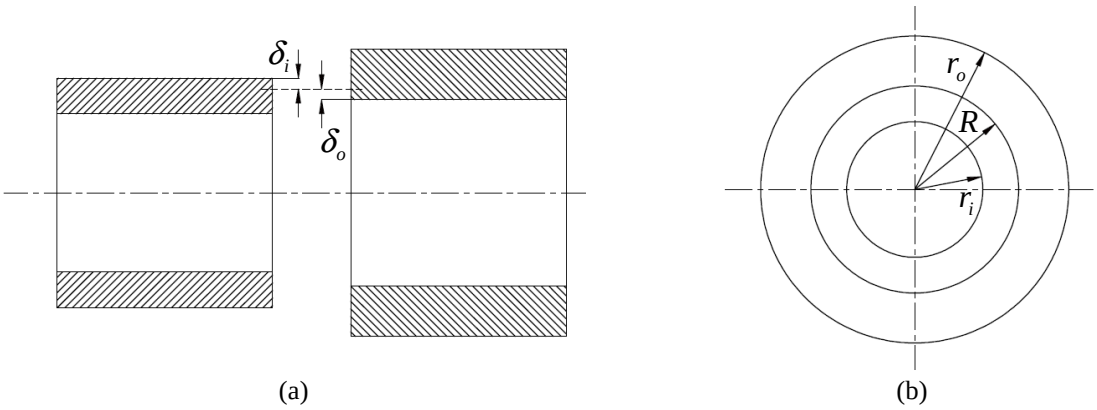

Figure 1. Assembly of two hollow cylinders by interference. (a) lateral sectioned view in the disassembled situation and (b) top view after assembly.

The tangential deformation in the external cylinder on the contact surface is

$$(\varepsilon_t)_o = \frac{2\pi(R + \delta_o) - 2\pi R}{2\pi R} = \frac{\delta_o}{R}. \tag{4}$$

Assuming a biaxial stress state, the tangential deformation in the external cylinder on the contact surface can be written as

$$(\varepsilon_t)_o = \frac{(\sigma_t)_o}{E_o} - \frac{\nu_o(\sigma_r)_o}{E_o}, \tag{5}$$

where E_o and ν_o are, respectively, the elastic modulus and Poisson coefficient of the external cylinder material, and $(\sigma_r)_o$ is the radial stress in the external cylinder on the contact surface.

Replacing Eq. (2) and Eq. (4) on Eq. (5) and knowing that $(\sigma_r)_o = -p$, one has

$$\delta_o = \frac{pR}{E_o}\left(\frac{r_o^{\,2} + R^2}{r_o^{\,2} - R^2} + \nu_o\right), \tag{6}$$

which is the equation for the change in the external cylinder radius on the contact surface. Similarly, the change in the internal cylinder radius will be

$$\delta_i = -\frac{pR}{E_i}\left(\frac{R^2 + r_i^{\,2}}{R^2 - r_i^{\,2}} - \nu_i\right). \tag{7}$$

Thus, Eq. (3) becomes

$$\delta = \frac{pR}{E_o}\left(\frac{r_o^{\,2} + R^2}{r_o^{\,2} - R^2} + \nu_o\right) + \frac{pR}{E_i}\left(\frac{R^2 + r_i^{\,2}}{R^2 - r_i^{\,2}} - \nu_i\right). \tag{8}$$

Equation (8) can be solved for the pressure when one knows the total radial interference value. This equation works for cylinders which have the same length. In the case of cylinders which have different lengths, an increase in the pressure value will occur on the contact surface borders. In this condition, it is usual apply a stress concentration factor. Its value depends on the contact pressure and the female element design, however, it is rarely greater than 2.

3. METHODOLOGY

The frame geometry is very complex and susceptible to errors descendent from the tooling process. Moreover, the stator core is a cylinder constituted by laminated plates, which has very low stiffness. These facts make the contact pressure estimation a redoubtable task, so estimating it accurately in a theoretical manner is almost impossible. An alternative way is to find its value in an indirect manner, by means of strain gauges installed on the external frame surface. The strains measured during the stator core insertion process are used in the finite element model calibration, that after convergence, provide the contact pressure between frame and stator core. Of course, this methodology requires that one knows the material properties of the frame and stator core. Besides, choosing the appropriated plasticity model helps in obtaining more accurate results. It is necessary also knowing the errors due to the frame tooling process. At this point, the dimensional control in measurement machines is fundamental.

3.1. Frame instrumentation

The frame instrumentation process was quite simple. Due to a limited number of measuring channels, four strain gauges were used. They were attached to one of the frame sides, because the frame has symmetry through the vertical plane. Figure 2 shows the strain gauges positioning. They are identified by the letters A, B, C and D. They were attached at 45° and -45° in relation to the horizontal axis and 160 mm from the frame borders, so that, they cover a considerable portion of the stator core length, which is centralized in relation to the frame. For the strain gauges attachment, it was necessary to make ditches on the frame surface. The ditches' depth had to be controlled in order to result a homogeneous thickness throughout the frame length. Despite only one of the frame sides has been instrumented, the tooling was done in both sides, to maintain the symmetry and similar stiffness in the whole frame circumference and to minimize the contribution of the tooling in the resulting strains.

As the interest was not obtaining the frame superficial stresses, unidirectional strain gauges were applied. The unidirectional strain at each strain gauge is enough for the finite element model calibration. After convergence, the finite element model provides indirectly, the radial stress on the contact surface between frame and stator core. Further stresses can also be obtained at any desired point of the model. The strain gauges were connected in a quarter bridge configuration using external dummies made in cast iron, the same material used in the frame. The dummies are shown in Fig. 3, which also shows one of the active strain gauges and the whole frame instrumented, moments before the stator core insertion process.

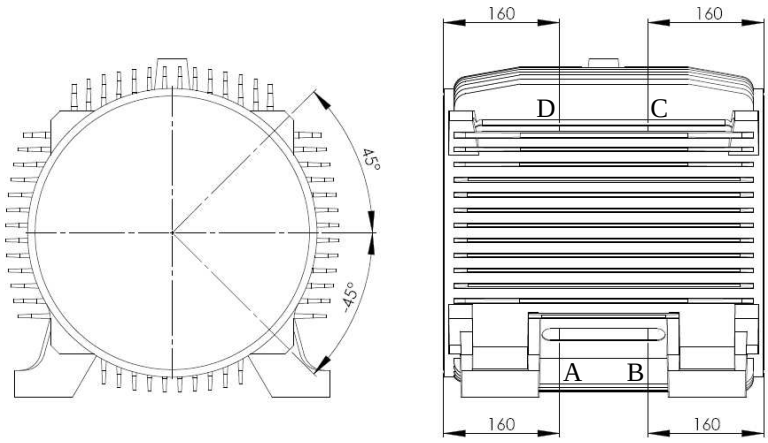

Figure 2. Strain gauges positioning on the frame.

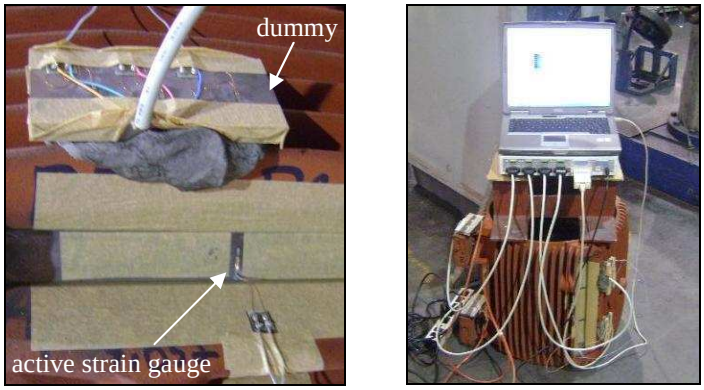

(a) (b)

Figure 3. Instrumented frame. (a) dummy and active strain gauge and (b) the whole frame.

3.2. Stator core insertion

The insertion of the stator core into the frame does not take so long. However, it demands attention, including regarding personal safety, because it involves handling the instrumented frame and signal acquisition system inside the plant. Another aggravating factor is the mass of the components. In this study, IEC 225 frames were used. It is in fact a quite big frame, which requires especial equipments for transportation, such as cranes, for example.

The insertion process is described as follows: initially, the stator core is placed into the press, on an especial base. Then, the frame is placed on the stator core and a metallic ring is put on the frame for receiving the press hammer. Next, a pre-insertion is done, in order to serve as a guide for the complete stator core insertion. Note that the small strains obtained at this stage are considered in the final strain computation. The next step is the complete stator core insertion, which must be a continuum process in order to guarantee the continuity of the strain curves obtained by the strain gauges. Figure 4 shows the frame and stator core in the press, ready for the insertion process and just after the process.

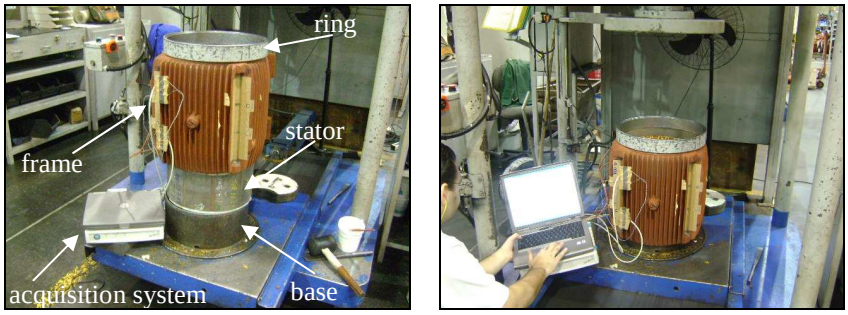

(a) (b)

Figure 4. Insertion of the stator core into the frame. (a) components before and (b) after insertion.

3.2. Finite element model

The finite element model (FEM) must represents with accuracy the real geometry and boundary conditions. Figure 5 and Fig. 6 present the CAD model for the frame and stator core as well as the corresponding FEM model. Note that it was modeled only one of the frame sides, because it has symmetry through the vertical plane, as previously attested. Besides, the Fig. 5 indicates the ditches that were done for the strain gauges placing. As can be seem in the figure, the strain gauges were represented by straight lines segments which have the same length as the real strain gauge foil. These lines were drawn inside the ditches, exactly in the same place where the real strain gauges were placed, in other words, at 45° and -45° related to the horizontal axis and 160 mm from the frame borders, as shown in Fig. 2. In order to investigate the strains in the stator core mid point, another straight line segment was drawn centralized between the two segments that represent the strain gauges, in both ditches. As the objective was not obtain the stresses in the frame feet and fins, but the radial stresses on the contact surface between the electric motor frame and its stator core, the feet and fins were modeled with bigger size elements than those used in the frame body mesh. Thus, one is able to reduce the processing costs without compromise the model response, since these components still contribute with the system stiffness.

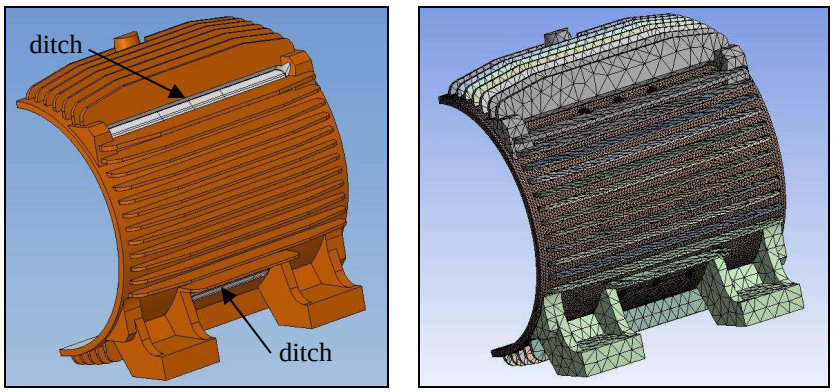

(a) (b)

Figure 5. Model external view. (a) CAD model and (b) FEM model.

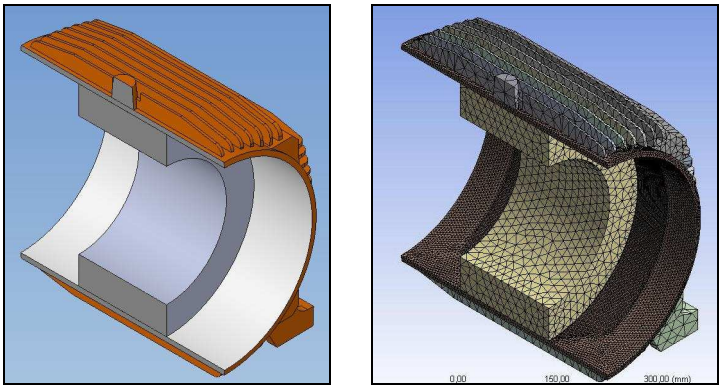

(a) (b)

Figure 6. Model internal view. (a) CAD model and (b) FEM model.

The stator core is made by laminated plates grouped by means of metallic clasps. For the purpose of this study, it was modeled as a hollow massive cylinder, neglecting the existence of the slots, meaning that only the yoke was considered. Following the same strategy used in the frame feet and fins, finite elements with bigger size were used in the stator core mesh. In the contact surface were used frictional type contact elements with friction coefficient of 0.2. This is the value for the friction coefficient between steel-steel. Because this is a non-linear contact type, it was chosen the stiffness matrix updating option for each iteration. This makes possible to get better convergence and results.

The interference was created in the CAD model. The first simulation was done based on theoretical values for the radial interference. After solution, the strain values obtained in the FEM model were confronted with the measured values. An iterative procedure took place until the convergence of these two values. At this point, the contact pressure value was estimated by the FEM along with the radial interference. About the restrictions, only the stator core axial displacement was fixed.

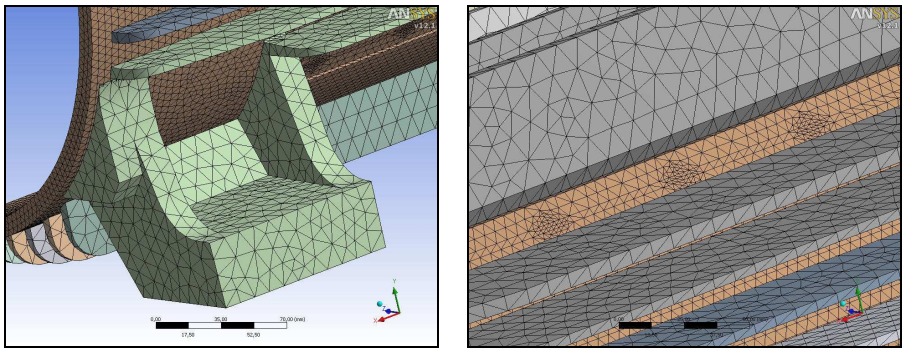

(a) (b)

Figure 7. Mesh details. (a) feet, fins and frame body (b) refinement at the strain gauges regions.

Figure 6 and Fig. 7 show the mesh refinement in the contact surface between frame and stator core and in the strain gauges regions. This refinement is necessary because at these points there is the interest in obtaining the radial stresses and strains, respectively. In order to obtain the radial stresses values and interferences and the strain gauges strains, two coordinate systems were created and are presented in Fig. 8. The first one is a Cylindrical coordinate system, which describes the radial stresses and interferences; the second is a Cartesian coordinate system rotated by 45° around the axial axis. This rotation makes two axis of the coordinate system parallel to the strain gauges strains directions.

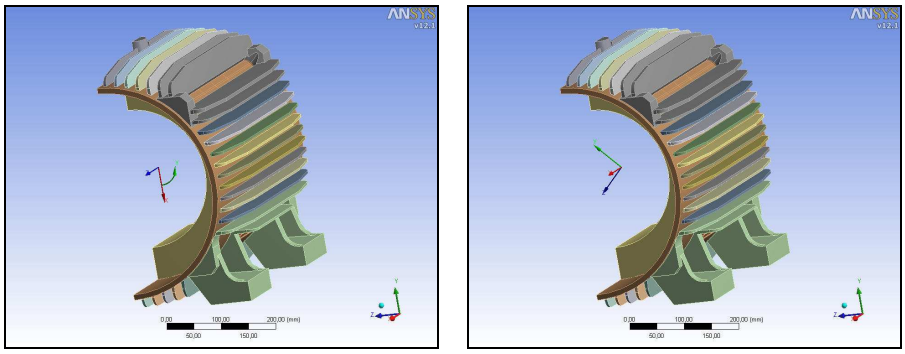

(a) (b)

Figure 8. Coordinate systems. (a) Cylindrical (b) Cartesian rotated by 45°.

3.3. Material models

As said before, the stator core is produced in ABNT 1006 Steel and the frame in FC-200 Cast Iron. These two materials have a very distinct behavior and must follow distinct material models. The steel has a linear behavior conducted by its elastic modulus. The cast iron behavior is more complex. For this material, it is necessary the adoption of a specific plasticity model. It is a two-phase material, graphite flakes inserted into a steel matrix. This microstructure leads to a substantial difference in behavior in tension and compression. In tension, the material is more brittle, with low strength and cracks form due to graphite flakes. In compression, no cracks were formed. The graphite flakes behave as an incompressible media that transmits stress and the steel matrix only governs the overall behavior. The adopted properties can be seen in Tab. 1. Note that for the cast iron, the finite element code was supplied also with the experimental curves in tension and compression.

Table 1. Mechanical properties for FC-200 Cast Iron and ABNT 1006 Steel.

	FC-200 Cast Iron	ABNT 1006 Steel
Elastic modulus, E [GPa]	90	211
Poisson coefficient, ν	0.24	0.30
Yield stress, σ_e [MPa]	-	220
Tensile ultimate stress, σ_{rt} [MPa]	200	420
Compressive ultimate stress, σ_{rc} [MPa]	600	-

The model assumes isotropic elastic behavior, and the elastic behavior is assumed to be the same in tension and compression. The plastic yielding and hardening in tension may be different from those in compression, as shown in Fig. 9.

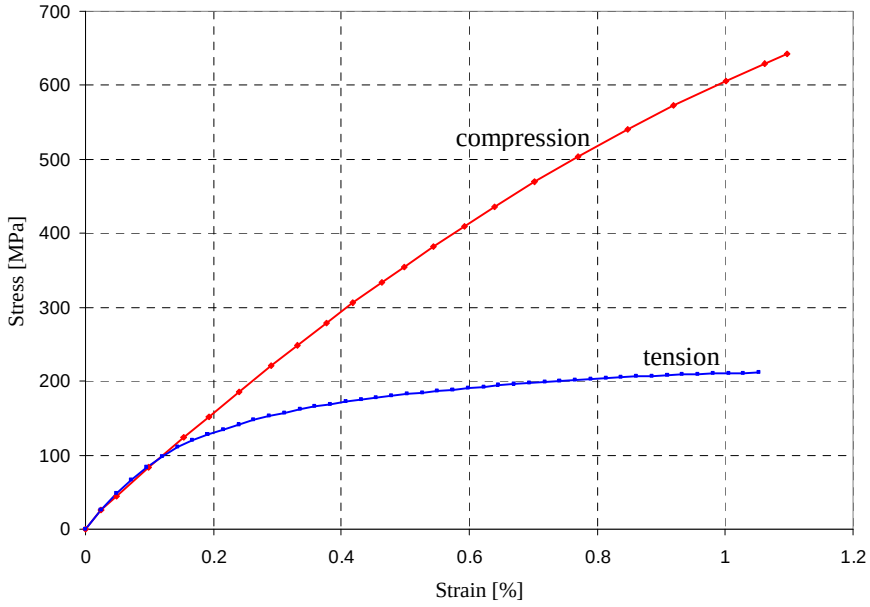

Figure 9. Stress-strain curves for FC-200 Cast Iron in tension and compression.

A composite yield surface is used to describe the different behavior in tension and compression. The tension behavior is hydrostatic pressure dependent and the Rankine maximum stress criterion is used. The compression behavior is hydrostatic pressure independent and the von Mises yield criterion is used.

The equivalent plastic strain is determined incrementally by a multilinear isotropic hardening model, such as the one shown in Fig. 10. In this model, the experimental data are supplied in a multilinear table form, where the first point defines the elastic modulus E, and the others, the various tangent elastoplastic modulus, $E_T's$ in the figure.

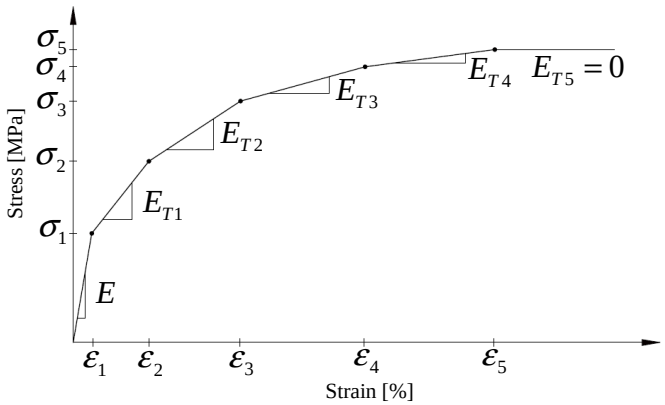

Figure 10. Multilinear isotropic hardening model.

4. RESULTS AND ANALYSIS

In order to evaluate the contact pressure behavior, two identical frames were prepared with distinct tooling dimensions in their internal diameters. In the first frame, identified as frame 1, the tooling was done to produce looseness in relation to the stator core. In the second one, identified as frame 2, the tooling was done to produce considerable interference in relation to the stator core. Theoretically, the medium radial interference value should be 0 mm for frame 1 and 0.4 mm for frame 2.

After the tooling process, the frames were measured, along with its stator cores. It was verified a medium radial looseness of 0.18 mm in frame 1 and a medium radial interference 0.41 mm in frame 2. It was also observed circularity errors of 0.91 mm and 0.84 mm for frames 1 and 2, respectively. These errors are due to the dispersion around the medium internal radius value in the frames. This dispersion achieved 0.20 mm in frame 1 and 0.27 mm in frame 2. Adding the internal radius dispersion value in frame 1 to the medium radial looseness in the same frame, one gets a radial interference of 0.02 mm. Similarly for frame 2, the resulting medium radial interference is about 0.68 mm.

Table 2 shows the theoretical and experimental obtained results for both frames, all in medium values. Note that, considering the dispersion, the estimated interference values by the finite element method were coherent. These interference values resulted in contact pressures values of about -0.61 MPa between frame 1 and its stator core and -14.45 MPa between frame 2 and its stator core. Table 2 also shows the medium strain values between the lower strain gauges, A and B, and the upper strain gauges, C and D. The finite element model solution procedure is iterative. It is done until the strain values in the FEM model agree with those obtained in the tests. For frame 1, the values obtained by the FEM for the upper strain gauges presented a good agreement. For the lower strain gauges, the values diverged of some about 355 %. For frame 2, it was achieved good equivalence for both, the upper and lower strain gauges. The maximum divergence was about 18 % for the upper strain gauges.

Table 2. Results for frames 1 and 2.

	Frame 1		Frame 2	
Strains A-B [1e-6m/m]	measured	FEM	measured	FEM
	38.5	129.0	2167.4	2167.3
Strains C-D [1e-6m/m]	measured	FEM	measured	FEM
	136.8	134.5	2764.8	2248.4
Estimated contact pressure [MPa]	-0.61		-14.45	
Estimated radial interference [mm]	0.021		0.78	

The explanation for the big error at the lower strain gauges is the tooling frame errors. The errors due to the tooling process vary throughout the frame length, resulting variations in the contact pressure value at each individual point. In fact, as can be seen in Fig. 11, the resulting strain in each strain gauge at the end of the stator core insertion process varies significantly. These variations are function of the cited errors. The finite element model does not consider the contribution of such errors by the moment, so that, the presented results are medium values between the upper and lower strain gauges.

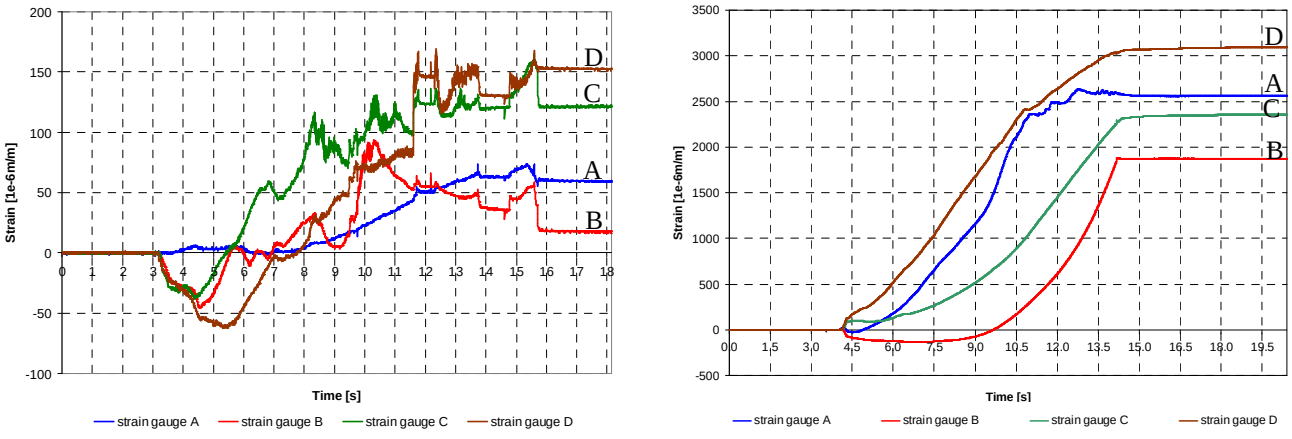

Figure 11. Strain gauges strains during the stator insertion process. (a) frame 1 e (b) frame 2.

The random behavior of the curves presented in Fig. 11 is due to shape errors in the internal diameter in both frames and to the superficial finishing after tooling. Figure 11 shows that frame 2, more tied than frame 1, is less susceptible to vibrations caused by superficial irregularities. Anyhow, the values used in this analysis are those obtained at the end of the stator core insertion process, i.e., the values corresponding to the time of 15.8 s, in the frame 1 curves, and 14.5 s, in the case of frame 2.

5. CONCLUSION

The methodology shown is quite useful in estimating the contact pressure value between frame and stator core of electric motors. This is the value of the compressive radial pressure resulting in the finite element model for the superficial frame strains obtained experimentally by means of strain gauges.

The contact pressure values can be related to the dynamic and thermal behavior of electric motors, so that, higher its value, lower the vibration levels in the equipment and better the thermal exchange rate. Investigate the relation between the contact pressure and the dynamic and thermal behavior of electric motors is theme for future papers.

The methodology is extremely sensible to any error descendant from the tooling process. Thus, mapping the shape and dimensional errors throughout the frame length and insert it into the model is useful to make the method more accurate and consequently, obtain better results. The refinement of the methodology can make possible describe the contact pressure gradient throughout the frame length. The dimensional control of the frames and stators are fundamental for the correct understanding and estimation of the pressure values.

6. ACKNOWLEDGMENTS

The authors are thankful to WEG Electric Equipments for supporting the prototypes and tests.

7. REFERENCES

Alger, P.L., “Induction machines”, New York: Gordon and Breach, 1970, pp. 376-377.

Ansys Reference Manual Release 13.0.

Associação Brasileira de Normas Técnicas, 1986. “NBR 6589: Peças em ferro fundido cinzento classificadas conforme a resistência à tração”, Brasil, 11 p.

Grante - Grupo de Análise e Projeto Mecânico, July 2004, “Extensometria: UFSC Course” (in portuguese), Mechanical Engineering Department, Federal University of Santa Catarina, Brazil, Course notes, 47 p.

Ishibashi, F.; Noda, S. and Mochizuki, M., 1998, “Numerical simulation of eletromagnetic vibration of small induction motor”, Proc. Inst. Elect. Eng. – Elect. Power Appl., Vol.145, pp. 528-534.

Ishibashi, F.; *et al*., 2010, “Change of mechanical natural frequencies of induction motor”, IEEE Transactions on Industry Applications, Vol.46, pp. 922-927.

Kester, W., 1999, “Practical design techniques for sensor signal conditioning”, Analog Devices, Inc., Norwood, Massachusetts, USA.

Knapp, J.; *et al*., 1998, “Measurement os shock events by means of strain gauges and accelerometers”, Elsevier Measurement Jornal, Vol.24, pp. 87-96.

Schlensok, C.; *et al*., 2008, “Structure-dynamic analysis of an induction machine on stator-housing coupling”, IEEE Transactions on Industry Applications, Vol.44, pp. 753-759.

Shigley, J.E; Mischke, C.R.; Budynas, R.G., 2005, “Projeto de engenharia mecânica”, Bookman, Porto Alegre, Brasil.

Simo, J.C. and Hugues, T.J.R., 1998, “Computational inelasticity”, Springer-Verlag Inc., New York, USA.

8. RESPONSIBILITY NOTICE

The authors are the only responsible for the printed material included in this paper.